Biogeosciences
Open Access

Discussions

Marine sources of bromoform in the global open ocean – global patterns and emissions

I. Stemmler[1,3], I. Hense[1], and B. Quack[2]

[1]Institute for Hydrobiology and Fisheries Science, University of Hamburg, CEN, Hamburg, Germany
[2]Geomar, Helmholtz Centre for Ocean Research, Kiel, Germany
[3]Max Planck Institute for Meteorology, Hamburg, Germany

Correspondence to: I. Stemmler (irene.stemmler@uni-hamburg.de)

BGD

11, 15693–15732, 2014

Bromoform in the open ocean

I. Stemmler et al.

Title Page

Abstract	Introduction
Conclusions	References
Tables	Figures

|◄ | ►|
◄ | ►

Back | Close

Full Screen / Esc

Printer-friendly Version

Interactive Discussion

Abstract

Bromoform ($CHBr_3$) is one important precursor of atmospheric reactive bromine species that are involved in ozone depletion in the troposphere and stratosphere. In the open ocean bromoform production is linked to phytoplankton that contains the enzyme
5 bromoperoxidase. Coastal sources of bromoform are higher than open ocean sources. However, open ocean emissions are important, because the transfer of tracers into higher altitude in the air, i.e. into the ozone layer, strongly depends on the location of emissions. For example, emissions in the tropics are more rapidly transported into the upper atmosphere than emissions from higher latitudes. Global spatio-
10 temporal features of bromoform emissions are poorly constrained. Here, a global three-dimensional ocean biogeochemistry model (MPIOM-HAMOCC) is used to simulate bromoform cycling in the ocean and emissions into the atmosphere using recently published data of global atmospheric concentrations (Ziska et al., 2013) as upper boundary conditions. In general, simulated surface concentrations of $CHBr_3$ match
15 the observations well. Simulated global annual emissions based on monthly mean model output are lower than previous estimates, including the estimate by Ziska et al. (2013), because the gas-exchange reverses when less bromoform is produced in non-blooming seasons. This is the case for higher latitudes, i.e. the polar regions and northern North Atlantic. Further model experiments show that future model studies may
20 need to distinguish different bromoform producing phytoplankton species and reveal that the transport of $CHBr_3$ from the coast considerably alters open ocean bromoform concentrations, in particular in the northern sub-polar and polar regions.

1 Introduction

Bromoform ($CHBr_3$) is one of the most abundant bromine containing volatile
25 halocarbon and is one considerable source for reactive bromine species in the atmosphere (e.g. Carpenter and Liss, 2000; Law and Sturges, 2007; Salawitch, 2006).

Due to its life-time of approximately 3–4 weeks (Moortgat et al., 1993; Law and Sturges, 2007) it alters the bromine budget in both the troposphere and the stratosphere and can lead to ozone depletion with potential impacts on the radiation budget of the atmosphere and consequently on climate (Hossaini et al., 2010; Saiz-Lopez et al.,
5 2012). Troposphere–stratosphere transport of short lived volatile compounds (including bromoform) highly depends on the location of the emissions (Aschmann et al., 2009; Tegtmeier et al., 2012), thus the spatio-temporal quantification of emissions is essential for assessing its impact on atmospheric chemistry and climate. However, bromoform emissions are so far poorly constrained and represent a significant uncertainty in
10 global atmospheric chemistry models (Hossaini et al., 2013). Bromoform has both natural and anthropogenic sources. Anthropogenic sources (e.g. desalination or disinfection of water, e.g. Allonier et al., 1999) are thought to contribute only little to the global emissions (Quack and Wallace, 2003). In the marine realm bromoform production is linked to enzymatic activity of (vanadium) bromoperoxydase (Moore
15 et al., 1996; Paul and Pohnert, 2011; Wever and van der Horst, 2013), which is contained in both micro- and macroalgae. Bromoform synthesis in the open ocean is mainly related to phytoplankton (Moore et al., 1996; Lin and Manley, 2012). The exact mechanism of bromoform production by phytoplankton is not fully understood. Laboratory studies show that it may be linked to phytoplankton growth (e.g. for
20 diatoms, Moore 1996; Hughes, 2013). However, there is also evidence that $CHBr_3$ can be produced extracellularly when bromoperoxidase reacts with dissolved organic matter (DOM) followed by decay of DOM to $CHBr_3$ (Lin and Manley, 2012; Wever and van der Horst, 2013). Thereby, both bromoperoxidase and DOM could originate from phytoplankton, released during decomposition or via exudation. The amount of
25 bromoform produced varies for different phytoplankton species, though differences between typical open ocean microalgae, i.e. the coccolithophores (*Emiliana* and *Calcidiscus*) and diatoms (*Chaetoceros*) are rather small (within a factor of 2) (Colomb et al., 2008). These different phytoplankton groups show different global distribution (e.g. illustrated for picophytoplankton, coccolithophores, and diatoms in Buitenhuis

et al., 2012; Leblanc et al., 2012; O'Brien et al., 2013). In addition, open ocean bromoform may partly originate from coastal sources via lateral transport (Moore and Tokarczyk, 1993; Carpenter and Liss, 2000). In fact, the coastal sources can be much stronger than the open ocean source (Moore and Tokarczyk, 1993; Quack and Wallace, 2003; Carpenter et al., 2009; Liu et al., 2011). In these regions production occurs predominantly by macroalgae (Manley et al., 1992; Laturnus, 2001; Leedham et al., 2013). All these aspects are important to understand current open ocean concentrations and emissions, and to potentially project its future development under a changing climate. Here, we address the question of the impact of phytoplankton and lateral transport from the coast on open ocean bromoform concentrations. For this purpose we implement a refined version of the bromoform module of Hense and Quack (2009) into a global ocean general circulation model that includes a marine biogeochemistry model (MPIOM: Marsland et al., 2003, HAMOCC: Ilyina et al., 2013). In a suite of present-day equilibrium simulations we investigate the contribution of bulk phytoplankton, diatom and non-diatom phytoplankton to bromoform production, assess the relevance of $CHBr_3$ advection from the coast, and characterize emissions to the atmosphere based on simulated oceanic concentrations and observed atmospheric concentrations.

2 Material and methods

2.1 Bromoform module

We use the bromoform cycling module as presented in Hense and Quack (2009). At that time the model was used within the one-dimensional water column model GOTM (Umlauf et al., 2005) together with a simple NPZD-type ecosystem model tuned to represent conditions during the Meteor Cruise M55 in the Cape Verde region. Here, we use the module within the three-dimensional ocean general circulation model of the Max Planck Institute for Meteorology, MPIOM (Marsland et al., 2003) coupled to

Bromoform in the open ocean

I. Stemmler et al.

⏮ | ⏭

◀ | ▶

Back | Close

Full Screen / Esc

Printer-friendly Version

Interactive Discussion

the Hamburg Ocean Carbon Cycle Model, HAMOCC (Ilyina et al., 2013). Only mean features of the bromoform module and modifications to the parameterization will be presented; details on the original parameterizations can be found in Hense and Quack (2009).

Bromoform B (in mmol m^{-3}) in the model is updated at every time step following production, decay, advection, diffusion, and gas exchange with the atmosphere. The only bromoform production process considered in the current study is $CHBr_3$ production during phytoplankton growth. We do not consider bromoform synthesis linked to phytoplankton sinks, i.e. the extracellular production of bromoform. Hense and Quack (2009) implemented this process and did not find differences in $CHBr_3$ concentrations, because phytoplankton sinks are closely co-located with its sources. This is also the case in HAMOCC, thus large-scale features will be the same, despite moderate differences in timing of maximum bromoform production. As the biogeochemistry model does not resolve plankton functional groups, we can not directly calculate species-(or group-)specific bromoform production. However, the contribution of diatoms can be assessed indirectly from the availability of silicate, as done previously for fractionating carbon export production and for parameterizing dimethylsulfide production (Kloster et al., 2006; Ilyina et al., 2013). It is assumed that diatoms grow faster than other phytoplankton groups, thus whenever silicate is available diatoms are dominating, whereas residual plankton groups dominate under silicate limiting conditions. The bromoform production ratio β is derived from the bulk bromoform production ratio β_0:

$$\beta = \beta_0 \cdot \left(\frac{\text{fac1} \cdot \text{Si(OH)}_4}{K_{\text{phy}}^{\text{Si(OH)}_4} + \text{Si(OH)}_4} + \frac{\text{fac2} \cdot K_{\text{phy}}^{\text{Si(OH)}_4}}{K_{\text{phy}}^{\text{Si(OH)}_4} + \text{Si(OH)}_4} \right)$$

where $K_{\text{phy}}^{\text{Si(OH)}_4}$ denotes the half-saturation constant for silicate (Si(OH)_4) uptake. Different factors fac1 and fac2 for the relative contribution of diatoms and non-diatom phytoplankton are tested (see Sect. 2.2).

Full Screen / Esc

Bromoform degradation processes considered in the model are photolysis, halide substitution, hydrolysis, and bacterial degradation during nitrification. We omit degradation during remineralization of detritus in this study, because Hense and Quack (2009) show, that it leads to unrealistic accumulation of bromoform in the deep ocean. An increase of the degradation rate did not solve this issue, but led to too low subsurface maxima. With regard to degradation by ammonium oxidizing bacteria we introduce one modification. As it was shown for freshwater nitrifiers, that these bacteria can oxidize volatile halogenated organic compounds (including $CHBr_3$, see e.g. Sayavedra-Soto et al., 2010) during oxidation of ammonium hydroxylamine, it seems reasonable to exclude this process for low oxygen conditions. Therefore, a threshold of $[O_2] > 50 \, \mu mol \, m^{-3}$ for the occurrence of this process was implemented.

Hense and Quack (2009) represent halide substitution and hydrolysis as one first order decay process with a half life of 4.37 years. As both processes are strongly temperature dependent, and follow different kinetics, hydrolysis and halogen substitution are implemented in the current study as separate sinks. Hydrolysis is implemented as a first order decay process with a temperature dependent decay rate l_{hyd}:

$$S = l_{hyd}(T) \cdot B$$

Washington (1995) reviewed hydrolysis rates of organic halogens and suggested the following temperature dependence of the basic hydrolysis rate k_B in $mol \, min^{-1}$:

$$k_B = A_1 \cdot \exp\left(\frac{-E_A}{RT}\right)$$

with $A_1 = 1.23 \times 10^{17} \, mol \, min^{-1}$, $E_A = 107\,300 \, J \, mol^{-1}$, $R = 8.314 \, J \, K^{-1} \, mol^{-1}$ and T is the seawater temperature in K. The hydrolysis rate then follows from

$$l_{hyd} = k_B \cdot [OH^-]$$

where [OH⁻] is calculated from the dissociation product of water and the hydrogen ion concentration, which are part of the carbonate chemistry formulation in HAMOCC (which uses the formulation of Roy et al., 1993).

Also halide substitution is implemented as a first order degradation process with a temperature-dependent rate constant (l_{subst})

$$S = l_{subst}(T) \cdot B$$

The rate is chosen to vary exponentially and represents a half life of $\tau_{1/2} = 5$ years at 25 °C and $\tau_{1/2} = 74$ years at 2 °C (Geen, 1992).

$$l_{subst} = l_{ref} \exp \left(A_2 \cdot \left(\frac{1}{T_{ref}} - \frac{1}{T} \right) \right)$$

with $l_{ref} = 7.33 \times 10^{-10}$ s^{-1} at $T_{ref} = 298$ K, $A_2 = 12\,507.13$ K and T seawater temperature in K.

In Hense and Quack (2009) CHBr$_3$ gas exchange with the atmosphere is calculated from the two-film model assuming it is controlled by the water side:

$$F_{air-sea} = k_w \cdot \left(B - \frac{c_a}{H} \right)$$

Hence, the flux is calculated from atmospheric concentrations c_a, solubility (Henry's law constant H, Moore et al., 1995), bulk surface water concentrations (B), and a transfer velocity (k_w). We modified the description of the transfer velocity to (Nightingale et al., 2000):

$$k_w = (0.222u^2 + 0.33u) \cdot \sqrt{\frac{660}{Sc_{CHBr_3}}}$$

to resolve the temperature dependence of the Schmidt number Sc_{CHBr_3} (Quack and Wallace, 2003):

$$Sc_{CHBr_3} = 4662.8 - 319.45T + 9.9012T^2 - 0.1159T^3$$

2.2 Model setup

The model experiments were designed to assess different aspects of bromoform cycling (Table 1). Four experiments were designed to study bromoform synthesis by phytoplankton. All of these experiments use the climatological atmospheric concentrations of Ziska et al. (2013) as upper boundary conditions and resolve all other bromoform cycling processes as described above. The reference experiment *Ref* uses the constant bulk bromoform production ratio derived from a laboratory study with diatoms (Moore et al., 1996; Hense and Quack, 2009). For usage in HAMOCC it was converted from nitrogen to phosphorus units using a constant Redfield ratio (N : P = 16 : 1). Based on Colomb et al. (2008) we derive a factor of about 2 in the mean bromoform production rate between the groups of the open ocean microalgae, i.e. the coccolithophores (*Emiliana* and *Calcidiscus*) and the diatom (*Chaetoceros*). As almost nothing is known about other phytoplankton groups (e.g. little on Baltic cyanobacteria Karlsson et al., 2008, and nothing on flagellates) we test both, a lower and higher production ratio by diatoms and residual (non-diatom) phytoplankton. In the experiment *Dia* the production ratio by diatoms is modified to be half that of residual plankton, i.e. fac1 = 0.5 and fac2 = 1. In the experiment *NDia* the opposite is implemented, i.e. production by non-diatoms is reduced, fac1 = 1 and fac2 = 0.5. Additionally, an experiment (*Half*) was conducted in which the constant bulk production ratio is only half of that in *Ref*, to separate the impact of a pure reduction of the global rate from fractionation among phytoplankton groups.

To test the hypothesis that open ocean bromoform is produced at the coast and advected to the open ocean, we conducted two joint experiments. In both experiments we eliminate the production of bromoform by phytoplankton, while we use the same atmospheric boundary conditions as in *Ref*. In the first one (*Coast*) we use a prescribed bromoform concentration of 80 pmol L^{-1} in waters shallower than 200 m. We chose this artificial approach, as it is impractical to resolve coastal sources (i.e. macroalgae with tide depending bromoform release, release from benthic algae and seagrass) explicitly

in a global model with approximately 1.5° horizontal resolution (curvilinear grid). As a result of the constant atmospheric boundary conditions a flux from air to sea will take place, because no bromoform is produced offshore. To quantify this bromoform source to the ocean, we perform a second experiment without prescribed bromoform on the shelf, *Equi* (which stands for equilibrium with the atmosphere). The comparison of *Coast* and *Equi* allows us to assess the relevance of lateral transport of bromoform from the coast to the open ocean.

An additional experiment was performed to address the effect of variability in the atmospheric concentrations. The life-time of bromoform in air leads to a distinct seasonal cycle in atmospheric mixing ratios (e.g. Beyersdorf et al., 2010; Hossaini et al., 2013). The additional experiment, *Seas-at*, differs from *Ref* only by the atmospheric boundary conditions for bromoform gas-exchange. Here, a monthly mean annual cycle was imposed onto the atmospheric boundary conditions, which was derived from the annual cycle of surface ocean bromoform concentrations simulated in *Ref*. In particular, the ratio between seawater concentration monthly means and their annual mean was used to construct the monthly means of atmospheric concentrations from the climatological mean. We thereby assume for simplicity that dynamics of atmospheric bromoform are controlled by oceanic concentrations. This is possible when the ocean is oversaturated with $CHBr_3$ and $CHBr_3$ is not accumulating in air.

For all simulations the model was restarted from a 1000 year spin up under preindustrial conditions ($pCO_2 = 278$ ppm) followed by a 200 year spin-up under present-day conditions ($pCO_2 = 353$ ppm). Following these spin-ups the model experiments were run into steady state (starting from a constant $CHBr_3$ concentration of 0.01 pmol L^{-1}) and model results were analyzed for the last year of the simulation, when surface waters down to 500 m were in quasi-steady state. All experiment use NCEP 6 hourly forcing (Behringer and Xue, 2004) interpolated to the model time step of 72 min and monthly mean model output is analyzed. In the following whenever we use the term "model" we are referring to MPIOM-HAMOCC.

2.3 Observations

CHBr$_3$ observations are taken from the Supporting Information of Ziska et al. (2013), who extrapolate cruise data submitted to the HalOcAt data base (https://halocat. geomar.de) into a global gridded field of bromoform concentrations and calculate emissions. For the model evaluation we use the individual ship cruise data to avoid the influence of patterns arising from extrapolation of the sparse data matrix. Generally, observed data from a particular month are compared to modelled monthly means. The exact origin of the individual data can be identified from the supplemental information (SI) in Ziska et al. (2013). The gridded atmospheric mixing ratios from the robust fit method are used as boundary conditions for the model after conservative spatial interpolation onto the model grid.

The observation-based net primary productivity that will be used in the model evaluation was downloaded from http://www.science.oregonstate.edu/ocean. productivity/index.php (accessed in June 2014). It was calculated from NASA's SeaWIFS (Sea-viewing Wide Field-of-view Sensor) level 3 data (PAR and Chl a) and NOAA's AVHRR (Advanced Very High Resolution Radiometer) sea surface temperature for 1997–2009 using the Vertically Generalized Productivity Model (VGPM) (Behrenfeld and Falkowski, 1997).

3 Results and discussion

3.1 Simulated open ocean sources and sinks of bromoform

The aim of the study is to investigate the impact of planktonic production and lateral transport on bromoform surface concentration patterns and on gas-exchange with the atmosphere. The spatial distribution of bromoform in seawater reflects the balance between sources (production and uptake from the atmosphere) and losses via outgassing and degradation. In the experiments that include planktonic

production of bromoform (*Ref*, *Half*, *Dia*, *NDia*, *Seas-at*) large-scale structures of surface concentrations are controlled by this process: maxima occur in biologically productive regions (e.g. in upwelling regions) and minima are located in the oligotrophic subtropical gyres in the Pacific and Atlantic Ocean (Figs. 1a, d and 2a, d). A reduction of the bulk production ratio of bromoform relative to primary production (*Half*) leads to a reduction of bromoform concentrations almost everywhere, apart from regions with uptake of bromoform from the atmosphere (e.g. the Southern Ocean and the northern extratropics in the local summer seasons, Fig. 1c and f). Lower marine $CHBr_3$ production leads here to lower surface ocean concentrations during the phytoplankton bloom and thus a larger difference between seawater and atmospheric concentrations, thus enhanced uptake from the atmosphere, which in turn leads to higher surface seawater concentrations after the phytoplankton bloom. Similarly, differences between *Ref* and *Seas-at* are highest, where a strong seasonal cycle in production results in a strong seasonality of $CHBr_3$ surface concentrations and by construction of the seasonally varying atmospheric forcing field of *Seas-at*, e.g. in the extratropics (Figs. 1, 7b and f around 50° N). Higher than climatological mean atmospheric concentrations lead to a reduction of the flux, and subsequently higher seawater concentrations. A comparison of the experiments *Ref* and *Equi*, in which the only bromoform source is uptake from the atmosphere, reveals that uptake is particularly relevant in higher latitudes (Supplementary Fig. S1), where it can deliver more than 70 % of the bromoform in surface seawater (not shown). In the polar regions bromoform production in the model is very low, as primary production is limited by light availability even during summer, because of the sea ice. However, there are some uncertainties related to the production and concentrations of bromoform. Bromoform cycling in polar regions is not well captured in the model. First, this is because of the importance of uptake from the atmosphere. Our stand-alone ocean model is forced by extrapolated atmospheric bromoform concentrations from Ziska et al. (2013), where data from $CHBr_3$ measurements are sparse. Second, our model does not consider a potentially important source process: production within sea ice and subsequent discharge into

Bromoform in the open ocean

I. Stemmler et al.

Full Screen / Esc

Printer-friendly Version

Interactive Discussion

Bromoform in the open ocean

I. Stemmler et al.

Printer-friendly Version

Interactive Discussion

seawater during melting or by diffusion through brine channels (Mattson et al., 2012; Granfors et al., 2013).

As mentioned above, bromoform distribution patterns for the main part follow the patterns of primary productivity. In the experiments *Dia* and *NDia* a relative reduction of the bromoform production ratio for diatom (*Dia*) or residual phytoplankton (*NDia*) dominance by a factor of 2 was implemented. As a consequence of silicate availability the model predicts largest diatom abundances in the northern and southern extratropics (Fig. 2b and e) and non-diatom phytoplankton in the lower latitudes (Fig. 2c and f). This distribution of diatoms is in line with the one predicted by models with explicit implementation of functional phytoplankton groups (e.g. Gregg and Casey, 2007) or diagnosed from satellite retrievals (Bracher et al., 2009). Due to the setup the bromoform production in both experiments is lower than in the experiment *Ref*, and bromoform concentrations are consequently lower. Compared to the uniform reduction of the bulk production rate in *Half*, concentrations are of course higher in regions in which the phytoplankton group with the unchanged (i.e. not reduced) production ratio dominates (Fig. 2). As diatoms dominate in productive regions, the impact of reducing the bromoform production rate by diatoms on the global CHBr$_3$ inventory is similar to the impact of reducing the bulk production rate by the same factor (Table 2). When focusing onto certain regions though, differences in the two approaches become apparent, e.g. in lower latitudes where non-diatom species dominate and the bromoform production (and concentration) is hence higher in *Dia* than in *Half*.

Primary production depends on light, temperature, and nutrient availability. Therefore in some ocean regions, such as the oligotrophic subtropical gyres, where surface nutrient concentrations are very low, production maxima are located in intermediate waters (at approximately 50–80 m). In most open ocean regions though, bromoform production maxima in the model are located at the surface, i.e. within the mixed layer (Fig. 3). This suggests that seasonal mixing with deeper ocean layers, i.e. the dynamics of the mixed layer depth, play only a minor role in shaping the temporal evolution of

Printer-friendly Version

Interactive Discussion

bromoform surface concentrations. However, in regions with deep production maxima in summer, like the subtropical North Atlantic, the deepening of the mixed layer in winter mixes bromoform upwards and leads to surface maxima that do not correspond to surface production maxima (as described also in Hense and Quack, 2009).

5   The experiments *Coast* and *Equi* were designed to study lateral transport of bromoform from the coast to the open ocean within its life-time. The mean global $CHBr_3$ residence time in steady state in the experiments with planktonic production is approximately 200 days (Table 2). The global residence time does not reflect the local life time of bromoform at certain water depths or locations. At the global scale it
10   is dominated by gas exchange ($\tau \approx 250$ d, Table 2), the residence time with regard to degradation is much longer ($\tau \approx 1100$ d, Table 2). Thus, the life-time within the the mixed layer is much shorter than in the deeper ocean. However, it could be still long enough to allow for considerable transport of bromoform from the coast to the open ocean. In the experiment *Coast* bromoform is reset to a concentration of
15   80 pmol L^{-1} in waters shallower than 200 m at each model time step. The comparison between *Coast* and *Equi* allows for assessing the relevance of lateral transport, as *Equi* accounts for the contribution of uptake from air in pristine open ocean waters. As expected, lateral transport from shelf regions is particularly relevant in the Arctic surface ocean (Figs. 4c, f and 5), because of its hydrographic features (mediterranian
20   sea) and low outgassing at cold temperatures. In contrast, the surface concentrations in the open Pacific Ocean are least influenced by coastal bromoform. Our chosen value of 80 pmol L^{-1} is an arbitrary value, however it is more than 15 times higher compared to the mean open ocean concentration and therefore high enough to roughly represent the gradient between open ocean coastal regions. In comparison to *Ref* most open
25   ocean regions in the Atlantic and Pacific show lower surface concentrations in *Coast* (not shown). However, even at water depths deeper than 1500 m 10–30 % of the coastal value are reaching 10 % of the grid cells at the surface (Figs. 5 and 4c, f). Thus, in the Northern Atlantic, downstream of high coastal production a considerable fraction of open ocean surface concentrations may be attributed to lateral transport of bromoform.

3.2 Evaluation of simulated surface concentrations

3.2.1 Comparison of simulated and observed surface concentrations

The evaluation of simulated surface concentrations is clustered regionally, i.e. the Atlantic, the Pacific, the Southern Ocean, and the Arctic Ocean are discussed separately.

Atlantic Ocean

Simulated surface concentrations in the Atlantic show a distinct spatial and temporal pattern. The temporal coverage of bromoform observations does not allow an extensive evaluation of the temporal evolution of bromoform concentrations. The spatial coverage, however, is high enough to compare spatial, in particular latitudinal, features of the $CHBr_3$ distribution. Data from three cruises allow to evaluate the latitudinal gradient in the Atlantic: the *Polarstern* cruise Blast 2 (Butler et al., 2007), the *Polarstern* cruise ANT X/1 (Schall et al., 1997) which both cross the Atlantic from the Northeast (off the European and North African continents) to South America in boreal fall (October, November), and the *Polarstern* cruise ANT XVII/1 (Chuck et al., 2005) which lead off the African coast from the subtropical North to the South Atlantic in August. Roughly, both simulated and observed concentrations in fall show high bromoform levels in the extratropics ($3–10\,pmol\,L^{-1}$), a decrease towards the subtropics (approximately $1\,pmol\,L^{-1}$) and a peak at the equator (approximately $2\,pmol\,L^{-1}$) (Figs. S14 and S24). In comparison to the *Polarstern* Blast 2 cruise (Butler et al., 2007), the general distribution is well represented in all experiments with an open ocean bromoform source, but the model overestimates the peak at the equator (factor of 1.35–1.8 between model and observation), and concentrations at the secondary peak at 10–20° N (factor of 1.95–2.6 between model and observation), and concentrations close to the Patagonian shelf (factor of 2–3) (Fig. S6). There are observations of bromoform at the equator in the same season that show higher

bromoform levels (8–14 pmol L^{-1}, Quack et al., 2004). Both maxima (at the equator an in the subtropics) are caused by spatial primary production maxima triggered by nitrate availability. Our parameterization of CHBr$_3$ production strongly relies on the quality of simulated spatio-temporal distribution of primary production. Primary production

5 is not a primary target parameter of HAMOCC, which is designed to capture global features of the carbon cycle, e.g. it is configured to reproduce realistic organic carbon export rates. We simulate a global net primary productivity (NPP) of 59.3 Gt C yr^{-1}, which is in the range of published estimates (e.g. 52 Gt C yr^{-1}, Westberry et al., 2008, < 40 Gt C yr^{-1} $>= 60$ Gt C yr^{-1}, mean 51 Gt C yr^{-1}: between less than 40 Gt C yr^{-1}

10 and more than 60 Gt C yr^{-1}, mean 51 Gt C yr^{-1}, Carr et al., 2006). Observations of primary production are not available from the ship cruises when CHBr$_3$ was measured. Therefore we compare the simulated primary production to a NPP product derived from satellite-based ocean color data (details in Sect. 2.3) to evaluate bromoform production in more detail. Indeed, the simulated primary production exceeds the observed NPP

15 in locations of equatorial upwelling in boreal summer (Fig. S3f). However, direct comparison along the ship track of Blast 2 indicates that this overestimation is just slightly higher than the observed maximum (650 vs. 590 mg C m^{-2} d^{-1}) (Fig. S7). The secondary maximum close to 15° N is within the range of observed primary production. This indicates that either conditions during the cruise are not captured in this satellite-

20 based estimate or that the implementation of the production process as a linear function of plankton growth does not fully capture characteristics of bromoform production. Furthermore, our model experiments are designed to reflect present-day conditions in the open ocean rather than to represent historic conditions. In the experiments with a reduced bromoform production rate (*Half*, *Dia*, *NDia*) the simulated bromoform

25 concentrations (2–2.7 pmol L^{-1} vs. 3.6 pmol L^{-1} in *Ref*) in the northern subtropical Atlantic are slightly closer to observations, which are around 1.0 pmol L^{-1}. This is true also when looking into the broader latitudinal bands (Fig. S5); in all of 50° S–20° N, and 40–60° N bromoform seems to be better represented with a reduced production rate. The comparison between other individual ship cruises, e.g. MSM 18/3 (Fig. S12)

Full Screen / Esc

Printer-friendly Version

Interactive Discussion

and DRIVE (Fig. S10) shows that this method ((fractional) reduction of the production ratio) does not improve uniformly the model results. Thus both, primary productivity, production rate (and species composition) need to reflect the conditions during the cruise to obtain the best possible representation of bromoform distribution patterns.

Pacific

To evaluate bromoform in the Pacific we closer look at data from four cruises in the Eastern Pacific (Blast 1, Gas Ex 98, Phase 1-04, RB-99-06 Butler et al., 2007) and one cruise in the Western Pacific (TransBrom Ziska et al., 2013); overlaps exist. Simulated concentrations in the northern West Pacific in fall represent observations during RB-99-06 very well (between 2 and 10 pmol L^{-1}), apart from underestimations close to the coast (Fig. S32). In spring concentrations in the model along the same track (Gas Ex 98) are at some locations three times higher than observations (Fig. S28), likely because primary production is overestimated by the model (Fig. S29). Similar mismatches of simulated and observed concentrations due to too high primary production in the model show up also in the equatorial Pacific when comparing to Phase 1-04 (Figs. S30, S31) in spring/early summer. In the eastern tropical Pacific overestimations of the primary production can be linked to a commonly known weakness of most biogeochemistry models, the so-called "nutrient trapping" in the equatorial Pacific (details in Dietze and Loeptien, 2013), where too high nutrient concentrations at the surface lead to too high primary and export production. For both the northern and the equatorial east Pacific bromoform concentrations in fall and winter match observations well (Blast 1, Fig. S26 and Gas Ex 98, Fig. S28). As the CHBr$_3$ concentrations in spring during highest bromoform production were overestimated, the underestimation in later months indicates that the too strong source is compensated by a strong sink, e.g. strong outgassing. In the Western Pacific only data from the TransBrom cruise are available to compare simulated and observed concentrations. Simulated bromoform concentrations are almost identical in all experiments, and closely match observations in the open ocean. Close to the Indonesian Shelf simulated

Full Screen / Esc

Printer-friendly Version

Interactive Discussion

concentrations are underestimated compared to observations, probably because of macroalgae or other coastal sources, which are not implemented in the model.

Southern Ocean and Arctic

The comparison of HAMOCC simulated primary production to the one derived by the VGPM model shows that NPP is overestimated in austral summer (Fig. S3) and along several ship tracks (ADOX, CLIVAR01, SWEDARP). Representation of primary production in satellite-based estimates (including VGPM) is poor in the Southern Ocean (Strutton et al., 2012). However, the overestimation of NPP could also indicate shortcomings of the biogeochemistry model, e.g. that iron limitation is not strong enough, as iron is the limiting nutrient for phytoplankton growth in this region or too strong mixing in the physical model. For the Southern Ocean it is difficult to directly conclude from deviations between simulated and observed NPP to the quality of simulated bromoform. E.g. overestimations in NPP do not always go in line with an overestimation of bromoform concentrations (e.g. S44 for ADOX). Apparently other parameters such as mixing have a strong impact on concentration patterns, too. This can be also seen for SWEDARP (S38, Abrahamsson et al., 2004), where bromoform concentrations do not follow the pattern of primary productivity or chlorophyll in both model results and observations. However, there are also examples for a good model representation of observed bromoform concentrations and primary production, i.e. for BLAST3 (February–April) and CLIVAR01 (October–November) (140–250° E).

As noted in Sect. 3.1 production of bromoform within sea ice by ice algae is not represented in the model. Therefore, open ocean $CHBr_3$ concentrations downstream of melting sea ice and close to sea ice are likely to be underestimated. Furthermore, the contribution of uptake from the atmosphere to bromoform sources is large in polar regions (e.g. around the Antarctic Peninsula) and atmospheric boundary conditions rely on extrapolation of very sparse data. Therefore, we can not expect to simulate seawater bromoform concentrations in polar regions correctly. For this reason the evaluation of Southern Ocean bromoform concentrations is only of preliminary nature and the

Bromoform in the open ocean

I. Stemmler et al.

Back | Close

Full Screen / Esc

Printer-friendly Version

Interactive Discussion

detailed evaluation of bromoform concentrations in the Arctic is omitted. However, for completeness a figure showing bromoform concentrations in the Arctic compared to observations from a ship cruise in June 2002 can be found in the SI (Figs. S52 and S53).

5 Overall the model is capable to represent large-scale features of observed bromoform concentrations, considering that no tuning of the model was performed. Discrepancies mostly arise from regionally weak representation of primary production or insufficient representation of environmental conditions during the ship cruises in this non-historical present-day model configuration. Note that we compare monthly
10 mean model output to observations along ship tracks, which usually lasted a couple of weeks. We refrain from analysing temporally higher resolved model output, because the atmospheric bromoform concentrations used in the gas-exchange do not resolve such high temporal variability. Differences among the model experiments are often smaller than differences between model results and observations. The best match with
15 observations is achieved when either reducing the bulk bromoform production rate, or considering lower bromoform production by diatoms than by non-diatom species (Fig. 6).

3.3 Gas-exchange with the atmosphere

Simulated bromoform emissions follow a pronounced seasonal cycle, dictated
20 by seawater concentrations and meteorological conditions. High emissions ($>$ 1200 pmol m^{-2} h^{-1}) occur in regions of high bromoform production, i.e. in boreal winter (DJF) in the Southern Ocean (Fig. 7b and e), in boreal summer (JJA) in the Northern Pacific and the Atlantic Oceans (Fig. 7a and d). In the oligotrophic subtropical gyres in contrast, bromoform emissions are low, but still positive, i.e. into
25 air ($<$ 50 pmol m^{-2} h^{-1}). Tropical upwelling regions always show high emissions, as bromoform production is high all year. In the Southern Ocean and the northern North Atlantic emissions in local winter seasons, and Arctic emissions are characterized by net uptake from the atmosphere. In the latter two regions this feature persists also in the

annual mean. In the Southern Ocean, high emissions in summer compensate for the uptake in winter, and over the year the ocean is a net source to the atmosphere. Also at the global scale the open ocean is a bromoform source to the atmosphere, and delivers approximately $0.3\,\mathrm{Gmol\,CHBr_3\,yr^{-1}}$ (Table 3). The reversal of gas-exchange depending on season implies, that the choice of proper atmospheric boundary conditions is important for simulating realistic bromoform emissions with a stand-alone ocean model. Generally, simulated emissions are higher in the Southern Hemisphere than in the Northern Hemisphere extratropics (Fig. 8). Note, we chose a different unit here than in the residual discussion of gas-exchange to ease the comparison with the recent evaluation of $CHBr_3$ emission inventories by Hossaini et al. (2013), who show a similar figure. Zonal maxima are higher than $0.8 \times 10^{-13}\,\mathrm{kg\,m^{-2}\,s^{-1}}$ in the southern extratropics and $0.4 \times 10^{-13}\,\mathrm{kg\,m^{-2}\,s^{-1}}$ in the Tropics, which is in contrast to the often assumed distribution that shows largest emissions from the tropical oceans (Quack et al., 2004; Warwick et al., 2006; Sousa Santos and Rast, 2013). Lowest emissions are simulated in experiments *Half* and *Dia* due to the lower bromoform production (Table 2). In these experiments the relative contribution of the Northern and Southern Hemisphere to total emissions is similar. Compared to *Half*, emissions in the lower latitudes in *Dia* are higher, because of low diatom presence.

Previous estimates of global annual marine bromoform emissions range from 1.5 to 10.3 Gmol (Table 3), considering either both coastal and open ocean regions or treating them individually. Most of these global estimates (except Palmer and Reason, 2009) are derived from indirect methods. This means that either bromoform measured in the marine boundary layer during ship cruises is used to calculate local fluxes which are extrapolated to the global scale (Butler et al., 2007; Ziska et al., 2013) or emissions needed as boundary conditions in atmospheric modelling studies are constrained to lead to least deviation of simulated air concentrations from observations (e.g. Warwick et al., 2006; Liang et al., 2010; Sousa Santos and Rast, 2013). The latter so-called "top-down" approaches all follow the same concept; the global ocean is split into latitudinal bands for which different emissions are applied. The approaches

differ in the number and extent of these zones, the treatment of the Tropics and coastal regions, and the temporal resolution considered. As mentioned above Hossaini et al. (2013) performed a detailed evaluation of global bromoform emission inventories for atmospheric modelling. They include three top-down inventories (Warwick et al., 2006;

5 Liang et al., 2010; Ordóñez et al., 2012), and the bottom-up (based on observations in air and water) inventory by Ziska et al. (2013) (OLS method). They are able to reproduce most of the seasonality of bromoform atmospheric mixing ratios with these temporally invariant emissions, presumably because it is driven by photolytic degradation in air (Hossaini et al., 2013). The seasonality in our simulated emissions

10 sometimes encompasses a variation of more than a factor of 2. The impact of this seasonality onto the evolution of atmospheric mixing ratios needs to be tested in dynamic ocean–atmosphere coupling. In Hossaini et al. (2013) good agreement between observed and simulated atmospheric mixing ratios, in particular within the Tropics could be achieved when using the emission inventory by Ziska et al. (2013),

15 which was the lowest of the previous estimates (Table 3). Therefore, we will focus in the comparison of our results with previous estimates on this inventory. Our open ocean emissions are even lower than this observation-based estimate by Ziska et al. (2013). Our approaches differ in the oceanic concentrations that drive the saturation anomaly. Our simulated ocean concentrations represent the observations used in

20 the extrapolation by Ziska et al. (2013) well, with a tendency of overestimating seawater concentrations (Sect. 3.2.1). Global fluxes are for several reasons lower in our approach. First, because our model considers the seasonality of oceanic concentrations. Simulated concentrations match observations well, however they are often lower in the winter season, for which observations are rare. Furthermore, we

25 do not include (and do not intend to represent) coastal emissions, which are generally higher than open ocean emissions. Another reason why our global emissions are lower than the ones in Ziska et al. (2013), is that their high emissions often occur in locations where no data exist, where nevertheless higher emissions are calculated based on the extrapolation method, e.g. in the northern North Atlantic and in the subtropical

Bromoform in the open ocean

I. Stemmler et al.

Back | Close

Full Screen / Esc

Printer-friendly Version

Interactive Discussion

East South Pacific. Our emissions indicate uptake from the atmosphere in the northern North Atlantic and the Gulf of Alaska and the Bering Sea in boreal winter (DJF), but fluxes into air in all other seasons, which leads to lower overall emissions. The only ship cruise in the subtropical east South Pacific is Blast 1, which does not show high

5 concentrations close to 30° S. Another region where our simulated fluxes deviate from the previous estimates are the subtropics. As primary production is low in subtropical gyres due to the nutrient limitation of plankton growth, $CHBr_3$ emissions are also low, approximately one third of the emissions by Liang et al. (2010) (compare Fig. 8 with Fig. 3 in Hossaini et al., 2013). Here, i.e. in the subtropical Atlantic, modelled

10 concentrations match observations well (e.g. compared to data from the Blast 2 cruise (Fig. S1, Butler et al., 2007), or data from the M60 cruise (Fig. S5, Ziska et al., 2013)). As gas exchange is the primary sink of ocean bromoform in in this region (Fig. 2b) we have confidence in the simulated emissions.

4   Conclusions

15 Our global coupled ocean biochemical model including bromoform is able to satisfactorily represent observed large scale patterns of bromoform surface concentrations in the open ocean. At the global scale, bulk phytoplankton based primary production appears to be a good proxy for simulating bromoform production in the open ocean. However at the regional scale, fractionation of bromoform synthesis

20 should be considered, with lower bromoform production by diatoms than by other phytoplankton groups. In the subarctic and Arctic regions bromoform formed in coastal regions can make a considerable contribution to open ocean bromoform concentrations. Bromoform emissions are characterized by large spatio-temporal variations, and only partly follow the latitudinal distribution patterns as suggested by

25 top-down approaches. The open ocean is a smaller source of bromoform than indicated by previous studies. Assuming similar vertical transfer in the atmosphere, the Pacific likely delivers more to the upper atmosphere than the Atlantic or Indian Ocean, as

Full Screen / Esc

Printer-friendly Version

Interactive Discussion

the model predicts highest emissions from the tropical Pacific compared to other low-latitude regions. Particularly interesting are the large-scale patterns that indicate bromoform uptake from the atmosphere, which do not show up in climatological mean emissions. In this regard bromoform production in polar regions needs to be refined in the model in future, especially because bromoform saturation ratios are close to equilibrium and may lead to seasonal reversal of gas-exchange. In addition to the global observation based emission climatology by Ziska et al. (2013) the simulated emissions describe realistic temporal features in the open ocean arising from bromoform production and thus can be used in atmospheric chemistry models that include bromine cycling.

The Supplement related to this article is available online at doi:10.5194/bgd-11-15693-2014-supplement.

Bromoform in the open ocean

I. Stemmler et al.

References

Abrahamsson, K., Bertilsson, S., Chierici, S., Fransson, A., Froneman, P., Lorén, A., and Pakhomov, E.: Variations of biochemical parameters alonga transect in the Southern Ocean, with special emphasis on volatile halogenated organic compounds, Deep-Sea Res. Pt. II, 51, 2745–2756, 2004. 15709

Allonier, A.-S., Khalanski, M., Camel, V., and Bermond, A.: Characterization of chlorination by-products in cooling effluents of coastal nuclear power stations, Mar. Pollut. Bull., 38, 1232–1241, doi:10.1016/S0025-326X(99)00168-X, 1999. 15695

Aschmann, J., Sinnhuber, B.-M., Atlas, E. L., and Schauffler, S. M.: Modeling the transport of very short-lived substances into the tropical upper troposphere and lower stratosphere, Atmos. Chem. Phys., 9, 9237–9247, doi:10.5194/acp-9-9237-2009, 2009. 15695

Behrenfeld, M. and Falkowski, P.: Photosynthetic rates derived from satellite-based chlorophyll concentration, Limnol. Oceanogr., 42, 1–20, 1997. 15702

Behringer, D. and Xue, Y.: Evaluation of the global ocean data assimilation system at NCEP: The Pacific Ocean, in: Eighth Symposium on Integrated Observing and Assimilation Systems for Atmosphere, Oceans, and Land Surface, AMS 84th Annual Meeting, Washington State Convention and Trade Center, Seattle, Washington, 11–15 January 2004, Session 2, Ocean Observations, Monday, 12 January 2004, available at: https://ams.confex.com/ams/84Annual/techprogram/paper_70720.htm, last access: 29 October 2014, 2004. 15701

Beyersdorf, A. J., Blake, D. R., Swanson, A., Meinardi, S., Rowland, F., and Davis, D.: Abundances and variability of tropospheric volatile organic compounds at the South Pole and other Antarctic locations, Atmos. Environ., 44, 4565–4574, doi:10.1016/j.atmosenv.2010.08.025, 2010. 15701

Bracher, A., Vountas, M., Dinter, T., Burrows, J. P., Röttgers, R., and Peeken, I.: Quantitative observation of cyanobacteria and diatoms from space using PhytoDOAS on SCIAMACHY data, Biogeosciences, 6, 751–764, doi:10.5194/bg-6-751-2009, 2009. 15704

Buitenhuis, E. T., Li, W. K. W., Vaulot, D., Lomas, M. W., Landry, M. R., Partensky, F., Karl, D. M., Ulloa, O., Campbell, L., Jacquet, S., Lantoine, F., Chavez, F., Macias, D., Gosselin, M., and McManus, G. B.: Picophytoplankton biomass distribution in the global ocean, Earth Syst. Sci. Data, 4, 37–46, doi:10.5194/essd-4-37-2012, 2012. 15695

Butler, J., King, D., Lobert, J., Montzka, S., Yvon-Lewis, S., Hall, B., Warwick, N., Mondell, D., Aydin, M., and Elkins, J.: Oceanic distributions and emissions of short-lived halocarbons,

Global Biogeochem. Cy., 21, GB1023, doi:10.1029/2006GB002732, 2007. 15706, 15708, 15711, 15713, 15724

Carpenter, L. and Liss, P.: On temperate sources of bromoform and other reactive organic bromine gases, J. Geophys. Res.-Atmos., 105, 20539–20547, 2000. 15694, 15696

Carpenter, L. J., Jones, C. E., Dunk, R. M., Hornsby, K. E., and Woeltjen, J.: Air-sea fluxes of biogenic bromine from the tropical and North Atlantic Ocean, Atmos. Chem. Phys., 9, 1805–1816, doi:10.5194/acp-9-1805-2009, 2009. 15696

Carr, M.-E., Friedrichs, M. A., Schmeltz, M., Aita, M. N., Antoine, D., Arrigo, K. R., Asanuma, I., Aumont, O., Barber, R., Behrenfeld, M., Bidigare, R., Buitenhuis, E. T., Campbell, J., Ciotti, A., Dierssen, H., Dowell, M., Dunne, J., Esaias, W., Gentili, B., Gregg, W., Groom, S., Hoepffner, N., Ishizaka, J., Kameda, T., Quéré, C. L., Lohrenz, S., Marra, J., Mélin, F., Moore, K., Morel, A., Reddy, T. E., Ryan, J., Scardi, M., Smyth, T., Turpie, K., Tilstone, G., Waters, K., and Yamanaka, Y.: A comparison of global estimates of marine primary production from ocean color, Deep-Sea Res. Pt. II, 53, 741–770, doi:10.1016/j.dsr2.2006.01.028, 2006. 15707

Chuck, A., Turner, S., and Liss, P.: Oceanic distributions and air–sea fluxes of biogenic halocarbons in the open ocean, J. Geophys. Res.-Oceans, 110, 1–12, 2005. 15706

Colomb, A., Yassaa, N., Williams, J., Peeken, I., and Lochte, K.: Screening volatile organic compounds (VOCs) emissions from five marine phytoplankton species by head space gas chromatography/mass spectrometry (HS-GC/MS), J. Environ. Monitor., 10, 325–330, 2008. 15695, 15700

Dietze, H. and Loeptien, U.: Revisiting "nutrient trapping" in global coupled biogeochemical ocean circulation models, Global Biogeochem. Cy., 27, 265–284, doi:10.1002/gbc.20029, 2013. 15708

Geen, C.: Selected Marine Sources and Sinks of Bromoform and Other Low Molecular Weight Organobromines, M.S. thesis, Dalhousie University, Halifax, Nova Scotia, Canada, 1992. 15699

Granfors, A., Karlsson, A., Mattsson, E., Smith, W. O., and Abrahamsson, K.: Contribution of sea ice in the Southern Ocean to the cycling of volatile halogenated organic compounds, Geophys. Res. Lett., 40, 3950–3955, doi:10.1002/grl.50777, 2013. 15704

Gregg, W. W. and Casey, N. W.: Modeling coccolithophores in the global oceans, Deep-Sea Res. Pt. II, 54, 447–477, doi:10.1016/j.dsr2.2006.12.007, 2007. 15704

Title Page

Abstract | Introduction

Conclusions | References

Tables | Figures

|◄ | ►|

◄ | ►

Back | Close

Full Screen / Esc

Printer-friendly Version

Interactive Discussion

Hense, I. and Quack, B.: Modelling the vertical distribution of bromoform in the upper water column of the tropical Atlantic Ocean, Biogeosciences, 6, 535–544, doi:10.5194/bg-6-535-2009, 2009. 15696, 15697, 15698, 15699, 15700, 15705

Hossaini, R., Chipperfield, M. P., Monge-Sanz, B. M., Richards, N. A. D., Atlas, E., and Blake, D. R.: Bromoform and dibromomethane in the tropics: a 3-D model study of chemistry and transport, Atmos. Chem. Phys., 10, 719–735, doi:10.5194/acp-10-719-2010, 2010. 15695

Hossaini, R., Mantle, H., Chipperfield, M. P., Montzka, S. A., Hamer, P., Ziska, F., Quack, B., Krüger, K., Tegtmeier, S., Atlas, E., Sala, S., Engel, A., Bönisch, H., Keber, T., Oram, D., Mills, G., Ordóñez, C., Saiz-Lopez, A., Warwick, N., Liang, Q., Feng, W., Moore, F., Miller, B. R., Marécal, V., Richards, N. A. D., Dorf, M., and Pfeilsticker, K.: Evaluating global emission inventories of biogenic bromocarbons, Atmos. Chem. Phys., 13, 11819–11838, doi:10.5194/acp-13-11819-2013, 2013. 15695, 15701, 15711, 15712, 15713

Ilyina, T., Six, K. D., Segschneider, J., Maier-Reimer, E., Li, H., and Núñez-Riboni, I.: Global ocean biogeochemistry model HAMOCC: Model architecture and performance as component of the MPI-Earth system model in different CMIP5 experimental realizations, J. Adv. Model. Earth Syst., 5, 287–315, doi:10.1029/2012MS000178, 2013. 15696, 15697

Karlsson, A., Auer, N., Schulz-Bull, D., and Abrahamsson, K.: Cyanobacterial blooms in the Baltic – a source of halocarbons, Mar. Chem., 110, 129–139, 2008. 15700

Kerkweg, A., Jöckel, P., Warwick, N., Gebhardt, S., Brenninkmeijer, C. A. M., and Lelieveld, J.: Consistent simulation of bromine chemistry from the marine boundary layer to the stratosphere – Part 2: Bromocarbons, Atmos. Chem. Phys., 8, 5919–5939, doi:10.5194/acp-8-5919-2008, 2008. 15724

Kloster, S., Feichter, J., Maier-Reimer, E., Six, K. D., Stier, P., and Wetzel, P.: DMS cycle in the marine ocean-atmosphere system – a global model study, Biogeosciences, 3, 29–51, doi:10.5194/bg-3-29-2006, 2006. 15697

Laturnus, F.: Marine macroalgae in polar regions as natural sources for volatile organohalogens, Environ. Sci. Pollut. R., 8, 103–108, 2001. 15696

Law, K. and Sturges, W.: Halogenated very short-lived substances, Chapter 2, in: Scientific Assessment of Ozone Depletion: 2006, WMO, Geneva, Report No. 50, 2007. 15694, 15695

Leblanc, K., Arístegui, J., Armand, L., Assmy, P., Beker, B., Bode, A., Breton, E., Cornet, V., Gibson, J., Gosselin, M.-P., Kopczynska, E., Marshall, H., Peloquin, J., Piontkovski, S., Poulton, A. J., Quéguiner, B., Schiebel, R., Shipe, R., Stefels, J., van Leeuwe, M. A.,

Varela, M., Widdicombe, C., and Yallop, M.: A global diatom database – abundance, biovolume and biomass in the world ocean, Earth Syst. Sci. Data, 4, 149–165, doi:10.5194/essd-4-149-2012, 2012. 15696

Leedham, E. C., Hughes, C., Keng, F. S. L., Phang, S.-M., Malin, G., and Sturges, W. T.: Emission of atmospherically significant halocarbons by naturally occurring and farmed tropical macroalgae, Biogeosciences, 10, 3615–3633, doi:10.5194/bg-10-3615-2013, 2013. 15696

Liang, Q., Stolarski, R. S., Kawa, S. R., Nielsen, J. E., Douglass, A. R., Rodriguez, J. M., Blake, D. R., Atlas, E. L., and Ott, L. E.: Finding the missing stratospheric Br_y: a global modeling study of $CHBr_3$ and CH_2Br_2, Atmos. Chem. Phys., 10, 2269–2286, doi:10.5194/acp-10-2269-2010, 2010. 15711, 15712, 15713, 15724

Lin, C. and Manley, S.: Bromoform production from seawater treated with bromoperoxidase, Limnol. Oceanogr., 57, 1857–1866, 2012. 15695

Liu, Y., Yvon-Lewis, S. A., Hu, L., Salisbury, J. E., and O'Hern, J. E.: $CHBr_3$, CH_2Br_2, and $CHClBr_2$ in US coastal waters during the Gulf of Mexico and East Coast Carbon cruise, J. Geophys. Res., 116, C10004, doi:10.1029/2010JC006729, 2011. 15696

Manley, S., Goodwin, K., and North, W.: Laboratory production of bromoform, methylene bromide, and methyl-iodide by macroalgaw in the nearshore southern California waters, Limnol. Oceanogr., 37, 1652–1659, 1992. 15696

Marsland, S., Haak, H., Jungclaus, J., Latif, M., and Röske, F.: The Max-Planck-Institute global ocean/sea ice model with orthogonal curvilinear coordinates, Ocean Model., 5, 91–127, 2003. 15696

Mattson, E., Karlsson, A., Smith, W., and Abrahamsson, K.: The relationship between biophysical variables and halocarbon distributions in the waters of the Amundsen and Ross Seas, Antarctica, Mar. Chem., 140–141, 1–9, 2012. 15704

Moore, R. and Tokarczyk, R.: Volatile biogenic halocarbons in the northwest Atlantic, Global Biogeochem. Cy., 7, 195–210, 1993. 15696

Moore, R., Geen, C., and Tait, V.: Determination of Henry's law constants for a suite of naturally occurring halogenated methanes in seawater, Chemosphere, 30, 1183–1191, 1995. 15699

Moore, R., Webb, M., Tokarczyk, R., and Wever, R.: Bromoperoxidase and iodoperoxidase enzymes and production of halogenated methanes in marine diatom cultures, J. Geophys. Res.-Oceans, 101, 20899–20908, doi:10.1029/96JC01248, 1996. 15695, 15700

Moortgat, G., Meller, R., and Schneider, W.: Temperature dependence (256–296 K) of the absorption cross sections of bromoform in the wavelength range 285–360 nm, in: The Tropospheric Chemistry of Ozone in the Polar Regions, Springer Berlin Heidelberg, 359–370, doi:10.1007/978-3-642-78211-4, 1993. 15695

Nightingale, P. D., Malin, G., Law, C., Watson, A., Liss, P., Liddicoat, M., Boutin, J., and Upstill-Goddard, R.: In situ evaluation of air–sea gas exchange parameterizations using novel conservative and volatile tracers, Global Biogeochem. Cy., 14, 373–387, 2000. 15699

O'Brien, L. M., Harris, N. R. P., Robinson, A. D., Gostlow, B., Warwick, N., Yang, X., and Pyle, J. A.: Bromocarbons in the tropical marine boundary layer at the Cape Verde Observatory – measurements and modelling, Atmos. Chem. Phys., 9, 9083–9099, doi:10.5194/acp-9-9083-2009, 2009. 15724

O'Brien, C. J., Peloquin, J. A., Vogt, M., Heinle, M., Gruber, N., Ajani, P., Andruleit, H., Arístegui, J., Beaufort, L., Estrada, M., Karentz, D., Kopczyńska, E., Lee, R., Poulton, A. J., Pritchard, T., and Widdicombe, C.: Global marine plankton functional type biomass distributions: coccolithophores, Earth Syst. Sci. Data, 5, 259–276, doi:10.5194/essd-5-259-2013, 2013. 15696

Ordóñez, C., Lamarque, J.-F., Tilmes, S., Kinnison, D. E., Atlas, E. L., Blake, D. R., Sousa Santos, G., Brasseur, G., and Saiz-Lopez, A.: Bromine and iodine chemistry in a global chemistry-climate model: description and evaluation of very short-lived oceanic sources, Atmos. Chem. Phys., 12, 1423–1447, doi:10.5194/acp-12-1423-2012, 2012. 15712, 15724

Palmer, C. and Reason, C.: Relationships of surface bromoform concentrations with mixed layer depth and salinity in the tropical oceans, Global Biogeochem. Cy., 23, GB2014, doi:10.1029/2008GB003338, 2009. 15711, 15724

Paul, C. and Pohnert, G.: Production and role of volatile halogenated compounds from marine algae, Nat. Prod. Rep., 28, 186–195, doi:10.1039/c0np00043d, 2011. 15695

Quack, B. and Wallace, D.: Air–sea flux of bromoform: controls, rates, and implications, Global Biogeochem. Cy., 17, 1023, doi:10.1029/2002GB001890, 2003. 15695, 15696, 15699, 15724

Quack, B., Atlas, E., Petrick, G., Stroud, V., Schauffler, S., and Wallace, D.: Oceanic bromoform sources for the tropical atmosphere, Geophys. Res. Lett., 31, 1–4, 2004. 15707, 15711

Roy, R. N., Roy, L. N., Vogel, K. M., Porter-Moore, C., Pearson, T., Good, C. E., Millero, F. J., and Campbell, D. M.: The dissociation constants of carbonic acid in seawater at salinities 5 to 45 and temperatures 0 to 45 °C, Mar. Chem., 44, 249–267, 1993. 15699

Saiz-Lopez, A., Lamarque, J.-F., Kinnison, D. E., Tilmes, S., Ordóñez, C., Orlando, J. J., Conley, A. J., Plane, J. M. C., Mahajan, A. S., Sousa Santos, G., Atlas, E. L., Blake, D. R., Sander, S. P., Schauffler, S., Thompson, A. M., and Brasseur, G.: Estimating the climate significance of halogen-driven ozone loss in the tropical marine troposphere, Atmos. Chem. Phys., 12, 3939–3949, doi:10.5194/acp-12-3939-2012, 2012. 15695

Salawitch, R.: Atmospheric chemistry: biogenic bromine, Nature, 439, 275–277, 2006. 15694

Sayavedra-Soto, L., Gvakharia, B., Bottomley, P., Arp, D., and Dolan, M.: Nitrification and degradation of halogenated hydrocarbons-a tenuous balance for ammonia-oxidizing bacteria, Appl. Microbiol. Biot., 86, 435–444, 2010. 15698

Schall, C., Heumann, K., and Kirst, G.: Biogenic volatile organoiodine and organobromine hydrocarbons in the Atlantic Ocean from 42° N to 72° S, Fresen. J. Anal. Chem., 359, 298–305, 1997. 15706

Sousa Santos, G. and Rast, S.: A global model study of natural bromine sources and the effects on tropospheric chemistry using MOZART4, J. Atmos. Chem., 70, 69–89, doi:10.1007/s10874-013-9252-y, 2013. 15711, 15724

Strutton, P., Lovenduski, N., Mongin, M., and Matear, R.: Quantification of Southern Ocean phytoplankton biomass and primary productivity via satellite observations and biogeochemical models, CCAMLR Sci., 19, 247–265, 2012. 15709

Tegtmeier, S., Krüger, K., Quack, B., Atlas, E. L., Pisso, I., Stohl, A., and Yang, X.: Emission and transport of bromocarbons: from the West Pacific ocean into the stratosphere, Atmos. Chem. Phys., 12, 10633–10648, doi:10.5194/acp-12-10633-2012, 2012. 15695

Umlauf, L., Burchard, H., and Bolding, K.: GOTM – scientific documentation: version 3.2, Marine Science Reports, 63, 1–346, 2005. 15696

Warwick, N. J., Pyle, J. A., Carver, G. D., Yang, X., Savage, N. H., O'Connor, F. M., and Cox, R. A.: Global modeling of biogenic bromocarbons, J. Geophys. Res.-Atmos., 111, D24305, doi:10.1029/2006JD007264, 2006. 15711, 15712, 15724

Washington, J. W.: Hydrolysis rates of dissolved volatile organic compounds: principles, temperature effects and literature review, Ground Water, 33, 415–424, doi:10.1111/j.1745-6584.1995.tb00298.x, 1995. 15698

Westberry, T., Behrenfeld, M. J., Siegel, D. A., and Boss, E.: Carbon-based primary productivity modeling with vertically resolved photoacclimation, Global Biogeochem. Cy., 22, GB2024 , doi:10.1029/2007GB003078, 2008. 15707

Wever, R. and van der Horst, M. A.: The role of vanadium haloperoxidases in the formation of volatile brominated compounds and their impact on the environment, Dalton T., 42, 11778–11786, doi:10.1039/C3DT50525A, 2013. 15695

Yokouchi, Y., Hasebe, F., Fujiwara, M., Takashima, H., Shiotani, M., Nishi, N., Kanaya, Y., Hashimoto, S., Fraser, P., Toom-Sauntry, D., Mukai, H., and Nojiri, Y., Correlations and emission ratios among bromoform, dibromochloromethane, and dibromomethane in the atmosphere, J. Geophys. Res., 110, D23309, doi:10.1029/2005JD006303, 2005. 15724

Ziska, F., Quack, B., Abrahamsson, K., Archer, S. D., Atlas, E., Bell, T., Butler, J. H., Carpenter, L. J., Jones, C. E., Harris, N. R. P., Hepach, H., Heumann, K. G., Hughes, C., Kuss, J., Krüger, K., Liss, P., Moore, R. M., Orlikowska, A., Raimund, S., Reeves, C. E., Reifenhäuser, W., Robinson, A. D., Schall, C., Tanhua, T., Tegtmeier, S., Turner, S., Wang, L., Wallace, D., Williams, J., Yamamoto, H., Yvon-Lewis, S., and Yokouchi, Y.: Global sea-to-air flux climatology for bromoform, dibromomethane and methyl iodide, Atmos. Chem. Phys., 13, 8915–8934, doi:10.5194/acp-13-8915-2013, 2013. 15694, 15700, 15702, 15703, 15708, 15711, 15712, 15713, 15714, 15724

Full Screen / Esc

Printer-friendly Version

Interactive Discussion

Table 1. Model experiments. All experiments consider the degradation processes described in Sect. 2.1.

	CHBr$_3$ production		Boundary conditions		
	Diatoms fac1	Non-diatoms fac2	Atmospheric CHBr$_3$ (c_a) climatological	monthly	Prescribed coastal CHBr$_3$ < 200 m 80 pmol L^{-1}
Ref	1.0	1.0	+	−	−
Dia	0.5	1.0	+	−	−
NDia	1.0	0.5	+	−	−
Half	0.5	0.5	+	−	−
Coast	0.0	0.0	+	−	+
Equi	0.0	0.0	+	−	−
Seas-at	1.0	1.0	−	+	−

Table 2. Simulated global annual bromoform production and loss ($Gmol\,CHBr_3\,yr^{-1}$), inventory ($Gmol\,CHBr_3$) and residence time (days).

Process	Clim-at	Seas-at	Half	Dia	NDia
Uptake	0.018	0.016	0.024	0.022	0.019
Outgassing	0.3142	0.311	0.149	0.22	0.24
Planktonic source	0.37	0.37	0.18	0.26	0.29
Inventory	0.215	0.205	0.1822	0.1966	0.200
Residence time (days)	205	197	322	253	241
	(249, 1141)	(239, 1124)	(445, 1167)	(326, 1144)	(304, 1161)

Table 3. Observation-based global annual bromoform net emissions (Gmol yr^{-1}) from the ocean.

| Source type	Lit. value	Reference
Open ocean	0.30,	Clim-at, Seas-at (net flux)
	10.01 (3–22)	Quack and Wallace (2003)
	10.26	Yokouchi et al. (2005)
	7.01	Warwick et al. (2006)
Global ocean	10.0	Butler et al. (2007)
Open ocean	1.9	Butler et al. (2007)
	7.45	Kerkweg et al. (2008)
	10.26	O'Brien et al. (2013)
Tropics	1.45	Palmer and Reason (2009)
Global ocean	5.3	Liang et al. (2010)
Open ocean	3.2	Liang et al. (2010)
	6.67	Ordóñez et al. (2012)
Global ocean	2.49	Ziska et al. (2013) (OLS)
Global ocean	1.5	Ziska et al. (2013) (RF)
Global ocean	3.5	Sousa Santos and Rast (2013)
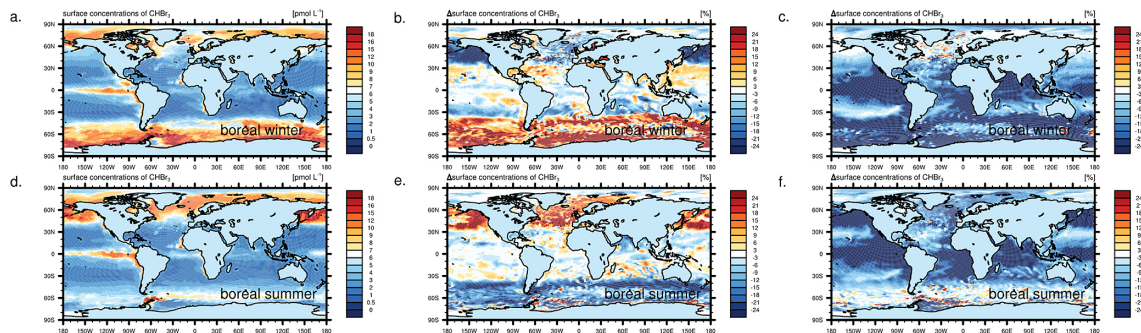
Figure 1. Mean surface bromoform concentrations ($pmol\,L^{-1}$) in experiment *Ref* in boreal summer **(a)** and boreal winter **(d)**, percentage difference (e.g. $100 \cdot \frac{Seas-at-Ref}{Ref}$) of *Seas-at* **(b, e)** and *Half* **(c, f)** in the same season.
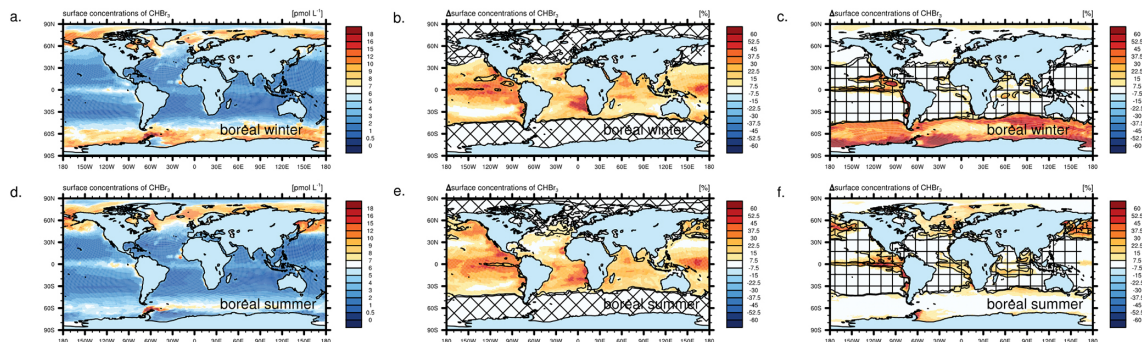
Figure 2. Mean surface bromoform concentrations ($pmol\,L^{-1}$) in experiment *Half* in boreal summer **(a)** and boreal winter **(d)**, percentage difference (e.g. $100 \cdot \frac{Dia - Half}{Half}$) of *Dia* **(b, e)** and *NDia* **(c, f)** in the same season. Contour lines show the fraction of diatoms **(b, e)** and non-diatoms **(c, f)** in bulk phytoplankton (0.5, 0.75, 1.0 contour lines), whereby fractions > 0.5 are indicated by a mesh pattern (inclined mesh for diatoms, straight mesh for non-diatoms).

Full Screen / Esc

Printer-friendly Version

Interactive Discussion
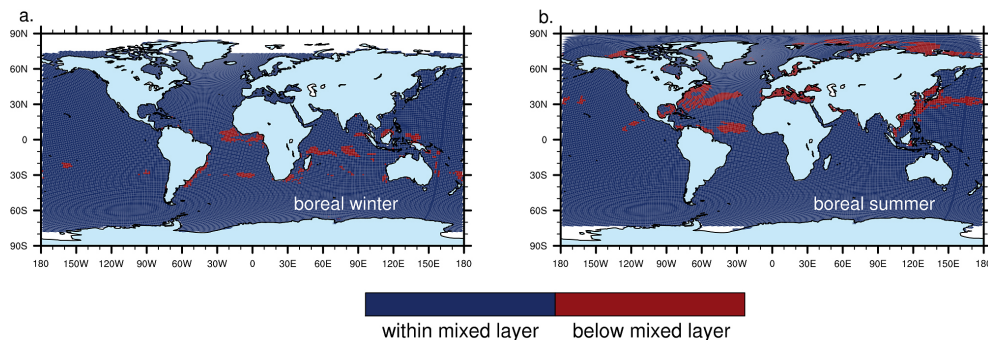
Figure 3. Location of bromoform production maxima in *Ref*: within or below mixed layer, boreal winter **(a)** and boreal summer **(b)**. The mixed-layer depth is defined as the depth, where a density (σ_T) difference of 0.125 relative to the surface value occurs.
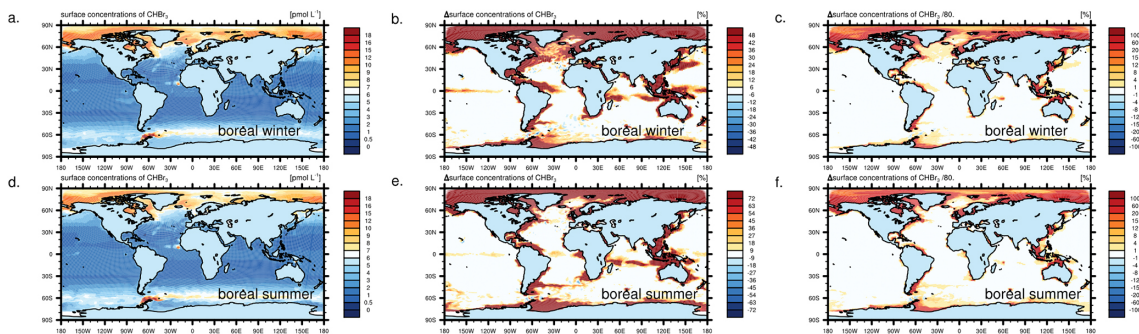
Figure 4. Mean surface bromoform concentrations ($\mathrm{pmol\,L^{-1}}$) in experiment *Equi* in boreal summer **(a)** and boreal winter **(d)**, percentage difference (e.g. $100 \cdot \frac{Coast - Equi}{Equi}$) of experiment *Coast* **(b, e)** and $100 \cdot \frac{Coast - Equi}{80\,\mathrm{pmol\,L^{-1}}}$ in the same season.
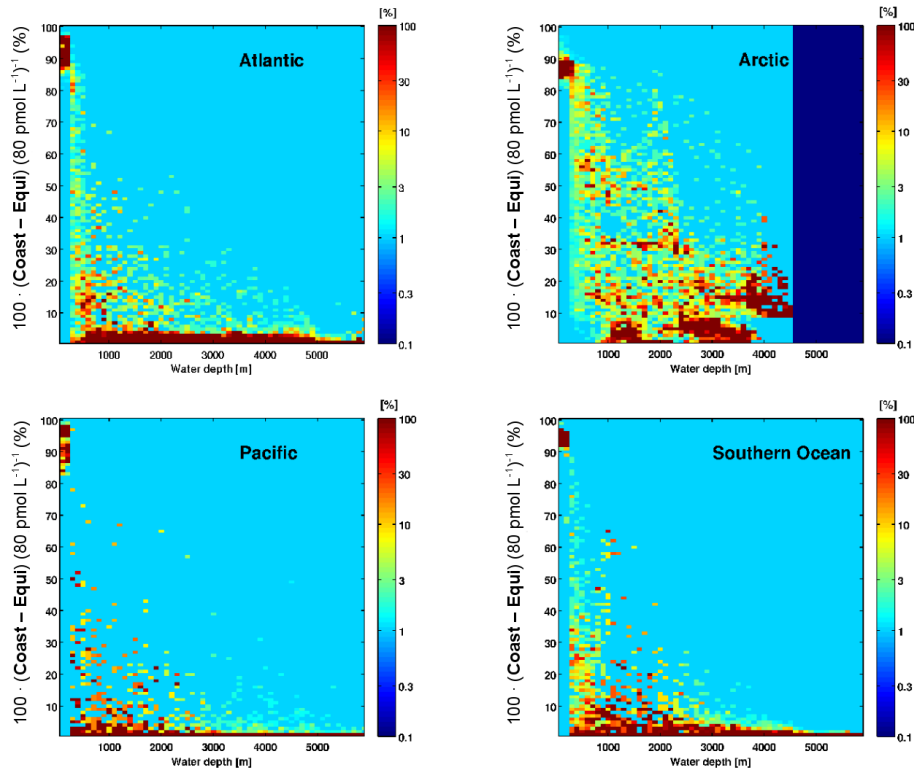
Figure 5. Histograms of $100 \cdot \frac{Coast - Equi}{80\,\mathrm{pmol\,L^{-1}}}$ surface concentrations [%] for different local water depths in the Atlantic, Arctic (upper row), Pacific, and Southern Ocean (lower row).

Full Screen / Esc

Printer-friendly Version

Interactive Discussion
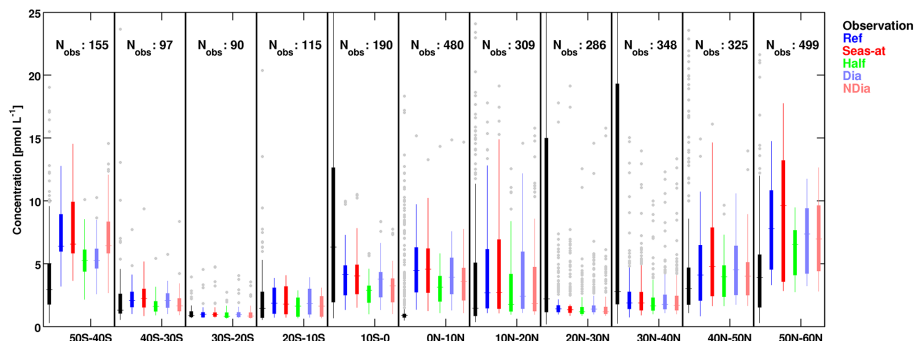
Figure 6. Box–Whisker plot of simulated and observed surface ocean bromoform concentrations (pmol L^{-1}). Box widths are determined by the 25 and 75 % percentile of data within each 10° latitude box, outliers (gray) are located outside 1.5 times the differences of the percentiles, the middle line of each box shows the median. Simulated concentrations are averaged over 1 grid cell around the location of observations. Different colors denote different experiments (*Ref*: blue, *Seas-at*: red, *Half*: green, *Dia*: pale purple, *NDia*: pale red); observations are shown in black.
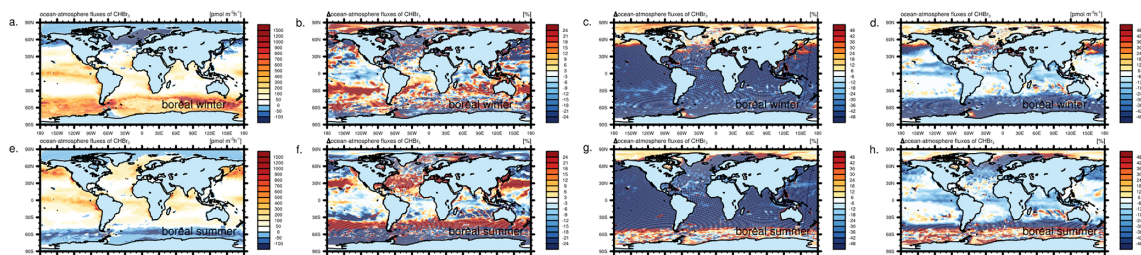
Figure 7. Mean bromoform sea–air flux (pmol m^{-2} h^{-1}) in experiment *Ref* in boreal summer **(a)** and boreal winter **(e)**, percentage difference (e.g. $100 \cdot \frac{Seas-at-Ref}{Ref}$) of *Seas-at* **(b, f)**, *Half* **(c, g)**, and *Dia* **(d, h)** in the same season.

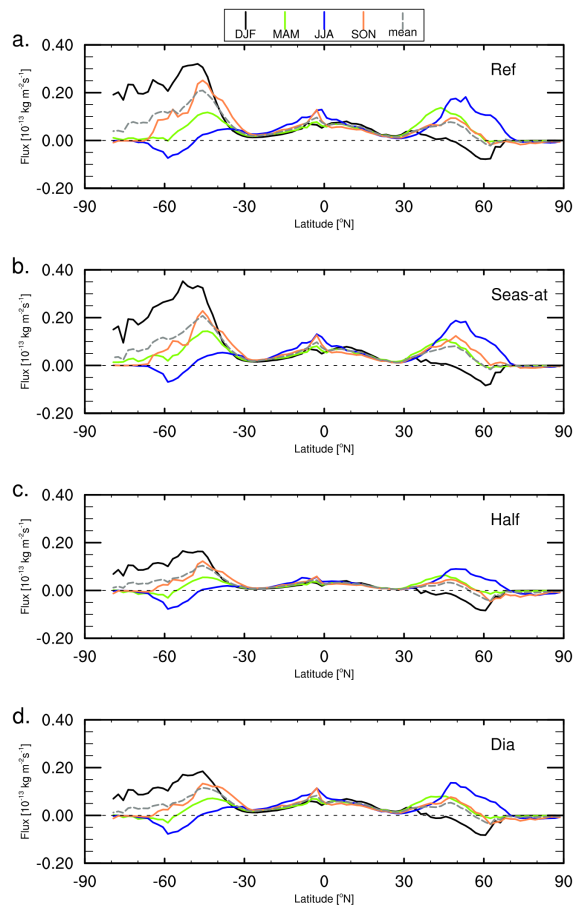Full Screen / Esc

Printer-friendly Version

Interactive Discussion

Figure 8. Zonal median of bromoform sea–air flux ($kg\,m^{-2}\,s^{-1}$), mean of JJA (blue), DJF (black), MAM (green), and SON (orange), and annual mean (dashed gray). Results are from *Ref* **(a)**, *Seas-at* **(b)**, and *Half* **(c)**, and *Dia*.